Turkish Journal of Chemistry

http://journals.tubitak.gov.tr/chem/

Research Article

Turk J Chem
(2022) 46: 1733-1743

doi:10.55730/1300-0527.3476

Insight into electrochemical degradation of Cartap (in Padan 95SP) by boron-doped diamond electrode: kinetic and effect of water matrices

Nguyen Tien HOANG
The University of Da Nang, University of Science and Education, Da Nang, Vietnam

Received: 08.02.2022 • **Accepted/Published Online:** 11.05.2022 • **Final Version:** 05.10.2022

Abstract: In this work, the kinetic electrochemical degradation of Cartap (CT) (in Padan 95 SP) at boron-doped diamond (BDD) electrode was investigated. This study indicated that the degradation of CT underwent both direct and indirect oxidations. Water matrices can either accelerate or inhibit the removal efficiency of CT: adding 15 mM Cl^- improved k_{CT} from 0.039 min^{-1} to 0.054 min^{-1} (increased by 38%), while k_{CT} decreased by 61.5% and 64% when increasing the concentration of HCO_3^- and humic acid (HA) to 15 mM and 15 mg L^{-1}, respectively. CT degradation was inhibited in the presence of methanol (MeOH) and *tert*-butanol (TBA) due to the scavenging effect of those chemicals toward reactive species. The contribution of reactive oxidants was calculated as: DET (direct electron transfer) accounted for 15%; •OH accounted for 61.5%; $SO_4^{\bullet-}$ accounted for 12.8%; ROS (the other reactive oxygen species) accounted for 8.5%. The transformation pathways of major reactive species were established.

Key words: BDD electrode, Cartap degradation, mechanism, kinetic, cyclic voltammetry, linear sweep voltammetry

1. Introduction

Pesticide is a toxic chemical substance, which usually contains more than two agents (including biological compounds) which are added into pesticide to control fungal or animal pests. However, due to the uncontrolled applications or the overuse of pesticides, the environment was seriously polluted. Depending on the chemical property, some pesticides can exist in the environment with different lifetime (from several days to several month and even e few decades). In some areas, the concentration of pesticides in agricultural wastewater is up to 500 mg L^{-1} that causes the serious environmental pollutions [1,2].

The powerful treatment methods should be developed and applied to decompose these polluted chemicals. To solve this urgent issue, the advanced oxidation processes (AOPs) are considered as an effective method to successfully remove none-biological degraded compounds from water, for example, ozonation, Fenton/photo-Fenton and photocatalysis processes [3,4]. However, the above methods have some disadvantages: ozonation requires the complicated equipment with high operating and maintenance costs [5]; Fenton/photo-Fenton discharges the high concentration of anions in the treated solution and large amounts of sludge; the low removal efficiency of photocatalysis process can be attributed to the low adsorption possibility of organics on the TiO_2 and the aggregation of TiO_2 because of the instability of the nanosized particle [6]. The electrochemical oxidation (EO) process is a promising technique to treat wastewaters containing toxic, refractory organic pollutants [7]. In EO process there are two possible mechanism pathways that involve in organics degradation: (1) direct oxidation in which the organic is directly oxidized thanks to the electron transfer on the anode surface; (2) indirect oxidation where various oxidizing species (i.e. •OH, $SO_4^{\bullet-}$, •OOH or H_2O_2, O_3, singlet oxygen, $O_2^{\bullet}$). In addition, other related electrolyte species also contribute to the organic decomposition [8]. The description of the interaction between oxidizing species and target compounds for both mechanism ways (direct and indirect oxidation) can be simplified in Eq. (1):

$$\text{Organic} + e^- / (\bullet OH / SO_4^{\bullet-} / \bullet OOH / O_3 / O_2^{\bullet}, \ldots) \rightarrow \text{intermediates} + CO_2 + H_2O + \text{inorganic ions} \quad (1)$$

* Correspondence: nthoang@ued.udn.vn

BDD is incapable of absorbing organics (see Text S1 and Figure S1 for more details) and a nonactive anode, which can react with H_2O to produce the physisorbed •OH (BDD(•OH)) (Eq. (2)), rending the organics degradation (Eq. (3)). The $SO_4^{\bullet-}$ (Eq. (4)) also contributes to the degradation of organics.

$$BDD + H_2O \rightarrow M(\bullet OH) + H^+ + e^- \quad (2)$$

$$BDD(\bullet OH) + R \rightarrow BDD + CO_2 + H^+ + e^- \quad (3)$$

$$S_2O_8^{2-} \rightarrow 2SO_4^{\bullet-} + 2e^- \quad (4)$$

Herein, this work reported the degradation of CT (in Padan 95SP) on BDD electrode. The BDD electrode was selected in this study because it performs very good electrochemical capability (high stability, resistance to corrosion, high overpotential for oxygen evolution) [9–[10]11]. Padan 95SP was selected for the degradation in EO process because of its widespread use in pest control in Vietnam.

The kinetic degradation of CT can be expressed as:

$$-\ln\frac{[CT]_0}{[CT]_t} = k_{CT}t = (k_{\bullet OH,CT}[\bullet OH]_{ss} + k_{SO_4^{\bullet-},CT}[SO_4^{\bullet-}]_{ss} + k_{ROS} + e^-)t \quad , \quad (5)$$

where k_{CT} represents the first-order rate constant of CT in the EO process, min^{-1}; $k_{\bullet OH,CT}$ and $k_{SO_4^{\bullet-},CT}$ the second-order rate constant of CT toward •OH and $SO_4^{\bullet-}$, respectively, $(M^{-1}\,s^{-1})$; k_{ROS} and e^- represent the first-order rate constant of CT by ROS and DET, (min^{-1}); $[\bullet OH]_{ss}$ and $[SO_4^{\bullet-}]_{ss}$ are the steady-state concentrations of •OH and $SO_4^{\bullet-}$, respectively (M).

The purpose of this study was to: (1) investigate the direct and indirect oxidation of CT in EO process; (2) study the effect of water matrices on CT removal efficiency; (3) insight into the contribution of radicals to the degradation of CT.

2. Materials and methods

2.1. Chemicals

Commercial pesticide Padan 95SP (95% CT) was purchased in Vietnam. Ellman's reagent (DTNB, 5,5'-Dithiobis (2-nitrobenzoic acid)) was supplied by Sigma-Aldrich for estimating the concentration of CT in Padan 95SP at interval times of electrolysis. Other chemicals (i.e. glycerol, benzoic acid (BA, 99%), nitrobenzene (NB, 99%), MeOH (99%), TBA (99%), boric acid, sodium sulfate, etc.) were also supplied by Sigma-Aldrich and Merck. The stuck solutions were prepared using deionized ultrapure water (Seralpur Pro 90 C).

2.1. BDD characterization

The BDD electrode was characterized using scanning electron microscopy (SEM, JSM-IT200, Japan), equipped with energy-dispersive X-ray spectroscopy (EDX) to analysis the elemental composition. X-ray diffraction (XRD, D8 ADVANCE ECO, Germany) with Cu Kα radiation (0.154 nm) was also used to determine the crystal structure of BDD.

2.2. Electrolysis

The electrolysis was carried out at ambient temperature (22 °C) in undivided cell of 400 mL. A BDD was used as the working electrode, supplied from Neocoat (Switzerland). The exposed surface area of BDD was 3.8 cm^2, the diamond layer was about 2.5–3 μm. In all cases, a Platinum foil with the surface area of one side of 2 cm^2 and Ag/AgCl (saturated KCl) were used as counter and reference electrodes, respectively. To stir 250 mL electrolyte solution continuously during the process, a magnetic bar was implied. Before starting experiment the working and counter electrodes were washed in ultrasonic bath for 10 min to remove contaminants, and then washed again with ultrapure water. The pH values of solution was controlled by 1 M H_2SO_4 or 1 M NaOH using a pH meter. Each experiment was duplicated for verification.

Electrolysis experiments were conducted under galvanostatic control at the applied current density ranged from 10 to 40 mA cm^{-2} using IviumStat (5 A current compliance/10 V power supply). Linear sweep voltammetry (LSV) test was performed in the potential range of 0–2 V at scan rate of 50 and 100 mV s^{-1} in 0.05 M Na_2SO_4. For CVs tests, the BDD electrode was characterized electrochemically in 0.05 M Na_2SO_4 solution in the absence and in the presence of Padan 95 SP. The cyclic voltammetry (CV) curves for the BDD electrode were recorded between –2.0 V to 2.0 V (E^0 vs. SCE) at different scan rates, sample interval was 0.01 V. The LSVs and CVs tests were conducted using Metrohm Autolab installed by Nova 2.1.3 software for electrochemical interface. Electrochemical impedance spectroscopy (EIS) was determine using Metrohm Autolab to investigate the conductivity of BDD in 0.2 M H_2SO_4 under the frequency from 1×10^5 to 1×10^{-2} Hz at open circuit potential.

2.3. Analysis methods

The solution samples were withdrawn at the time intervals and immediately measured using DTNB procedure, which can be clearly described elsewhere [12,13]. This technique was based on the generated yellow anions (3-carboxy-4-nitrophenylthiolate anion), which were then determined at the maximum wavelength of 412 nm in a UV-Vis spectrophotometer (V730, Japan). The spectrum for CT determination can be seen in Text S2 and Figure S2.

The degradation efficiency of CT is calculated according to Eq. (6):

$$m = \frac{1-C}{C_0} \times 100\%, \quad (6)$$

where C is the remaining content of CT at a given electrolytic time and C_0 is the initial concentration.

The theoretical mineralization of CT is proposed in Eq. (7):

$$C_7H_{15}N_3O_2S_2 + 20H_2O \rightarrow 2SO_4^{2-} + 3NH_4^+ + 7CO_2 + 43H^+ + 42e^- . \quad (7)$$

The concentrations of BA and NB were measured by HPLC aligent 1200 (Germany) with C18 column (250 mm × 4.6 mm, 5 μm) coupled with a UV detector. The detection of BA and NB was performed at 227 and 270 nm, respectively, at a flow rate of 1 mL min^{-1}. The mobile phase of methanol/water (65:35) (v/v) contained 1 % phosphoric acid. The column temperature was 30 °C. Additionally, the concentration of BA and NB can be also calculated using UV-Vis (V730, Japan), because the formed byproducts and the presence of SO_4^{2-} did not cause any interferes for the detection of BA and NB at 224 nm and 270 nm, respectively (The HPLC/UV spectrum of BA/NB and the degradation of BA/NB during the EO process can be seen in Figure S3).

3. Result and discussion

3.1. BDD characterization and electrochemical properties

Due to the lack of information about this commercial BDD electrode, BDD was again characterized using SEM, XRD and EIS. As can be seen in Figure 1a, the BDD layer consists of the grains with the medium size of 200 nm. The orient of the grains was randomly grown on the substrate Si. According to EDX spectrum, some elements were detected, including C (71.5%), B (15.1%), O (11.8%), and Si (11.6%) (Figure 1b). Moreover, the phase of BDD can be proved by the diffraction peak at 2θ = 70.35°, which can be coincided with crystal planes of the hexoctahedral phase of diamond (diamond cubic) (Figure 1c). The roman spectrum and XPS of BDD can be clearly seen in our previous publication [10].

The impedance spectrum of BDD and its comparison with Ti and Pt are shown in Figure 2. The arc diameter of BDD was much smaller than Ti and higher than Pt electrodes, indicating that charge transfer resistance of those electrodes followed the order: Ti (35 kΩ) > BDD (92.6 Ω) > Pt (13 Ω) (use the electrochemical circle fit command in NOVA 2.1.3 software to calculate the resistance). The above result indicates that the BDD can be considered a good conductive electrode thanks to the BDD layer on Si substrate.

3.2. Cyclic voltammetry curve in absence and presence of Padan 95 SP

The electrochemical character of BDD electrode with SO_4^{2-} anion is an important factor to initially study the CT degradation mechanism in Na_2SO_4. The CV curves of BDD electrode under different conditions are depicted in Figure 3. Similar to previous study [14], we also found the oxidation peak **P1** occurring at the potential between 1 V and 1.3 V (Figure 3a), suggesting that the direct oxidation of CT can occur due to the electron transfer on the BDD surface. Generally, the oxidation peak potential must be less than the oxygen evolution potential (Eq. (8)), as also confirmed by M. Panizza and G. Cerisola [8]:

$$H_2O \rightarrow 4H^+ + 4e^- + O_2 \quad E^0 = 1.23\ V\ (E^0\ vs\ NHE) \quad (8)$$

When increasing the scan rate to 100 mV s^{-1}, the direct oxidation of CT was enhanced, as a result of the promotion of electron exchange at BDD surface. This is because the high scan rates provides high current density for shorter time frame, thereby increasing the oxidation current peak [15]. Therefore, the degradation of CT underwent both mechanisms: (1) direct oxidation via electron transfer at the surface of BDD; (2) the indirect oxidation by reactive radicals. The contribution of direct oxidation and indirect oxidation (via •OH, $SO_4^{\bullet-}$, etc.) were discussed in subsections 3.4 and 3.5.

In the negative potential, the reduction peak **P2** at –1.2 V is probably associated to the evolution of H_2 from H_2O and/or the formation of persulfate (Eqs. (9) and (10)). When increasing the scan rate to 100 mV s^{-1}, the intensity of the reduction peak increased.

$$SO_4^{\bullet-} + SO_4^{\bullet-} \rightarrow S_2O_8^{2-} \quad (9)$$

$$SO_4^{\bullet-} + SO_4^{2-} \rightarrow S_2O_8^{2-} + e^- \quad (10)$$

The further investigation of the scan rates at different concentrations of CT were illustrated in Figures 3b and 3c and there are no significant differences between two ranges of concentration, indicating that the degradation through direct oxidation is unchanged at high CT concentration.

In addition, the effect of current density on O_2 evolution and CT degradation can be found in detail in Texts S3 and S4, Figures S4–S6.

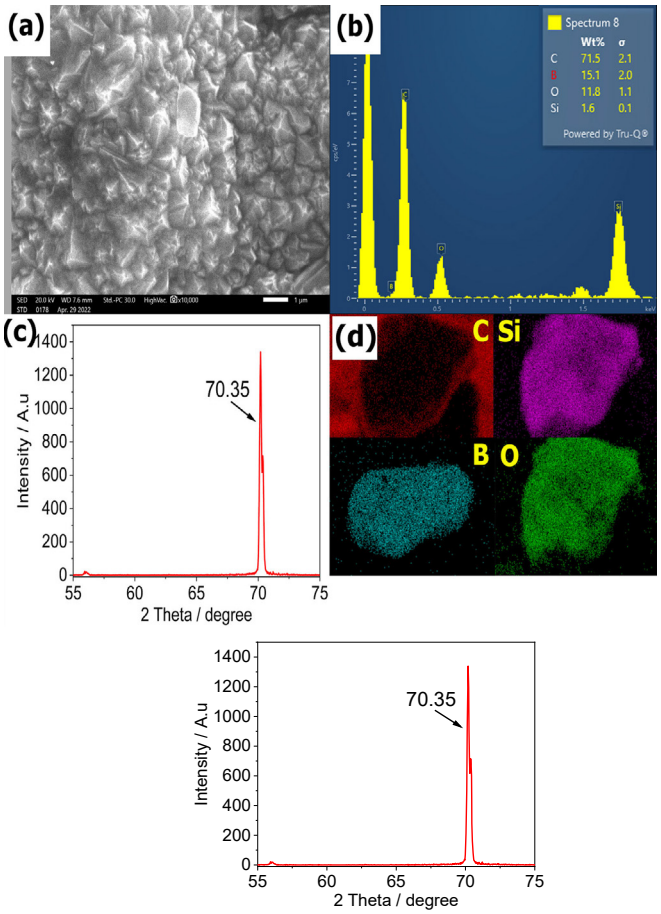

Figure 1. Elemental analysis for BDD electrode. a) SEM image of BDD; b) EDX for detecting elements; c) XRD patterns of the BDD electrode; d) Detected elements on BDD.

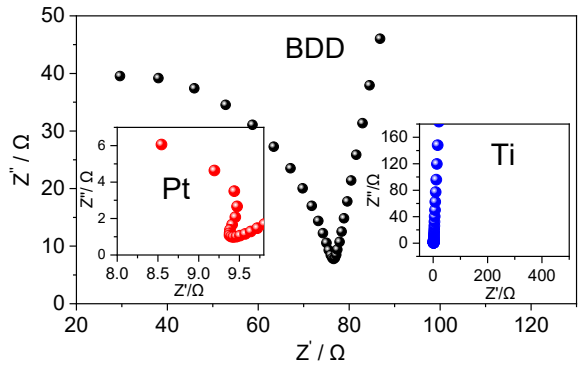

Figure 2. EIS spectrum of BDD. Inert: EIS spectrum of Pt and Ti.

3.3. Effect of different water matrices

Some anions (i.e. HCO_3^-/CO_3^{2-}, Cl^-, Fe^{2+}, NO_3^-, etc.) and humic acid (HA) can be found in natural water. In this study, HCO_3^- and Cl^- were selected because they are common anions in water. HA was chosen because it represents the organic matter in natural water. Their presence affects the degradation efficiency of organics during the process. The formation of radicals and their transformation in the presence of water matrices can be listed in Table S2. Therefore, the effects of HCO_3^-, Cl^- and HA on CT removal were investigated, as shown in Figure 4.

Effect of HCO_3^-: k_{CT} (the first-order rate constant for CT) decreased from 0.039 min^{-1} to 0.014 min^{-1} (decreased by 74%) when increasing HCO_3^- concentration from 0 to 15 mM (Figure 4a). This result could be attributed to the scavenging effect of bicarbonate toward •OH and $SO_4^{\bullet-}$ (Reactions (82) and (83), Table S2). This scavenging effect leads to the formation of $CO_3^{\bullet-}$ with weaker oxidation capability (their reaction rate constant toward organics is in the range of 10^{-6}–10^{-7} M^{-1} s^{-1}, Table S2), thereby reducing the removal efficiency of process. As a result, CT removal decreased from 68% to 32% after 30 min when increasing HCO_3^- concentration from 0 to 15 mM (Figure 4b).

Effect of Cl^-: k_{CT} increased from 0.039 min^{-1} to 0.054 min^{-1} (increased by 1.4 folds) when increasing Cl^- concentration from 0 to 15 mM (Figure 4c). The removal efficiency increased from 68% to 81% after 30 min as increasing Cl^- concentration to 15 mM (Figure 4d). The presence of chloride ion can enhance the CT removal due to some aspects: (1) Cl^- could be oxidized by electrolysis to produce active chlorine and/or chloride radicals (ClO^-/Cl•) [16,17]. The oxidation capability of Cl• toward organics is comparable to •OH (in the range of 10^9–10^{10} M^{-1} s^{-1}. Table S2), thereby contributing to the degradation of CT; (2) Cl^- reacts with •OH and $SO_4^{\bullet-}$ to produce reactive chlorine species (RCS: Cl•, $Cl_2^{\bullet-}$, $ClOH^{\bullet-}$, etc) (Reactions 35–80, Table S2) which could also enhance the removal efficiency of CT in the electrolysis process. Despite the fact that the scavenging effect of Cl^- lead to decreased concentration of $SO_4^{\bullet-}$, the significant formation of RCS at high concentration of Cl^- might compensate the fade of $SO_4^{\bullet-}$, leading to the improvement of process. The same results can be observed in other AOPs [18–21], where the kinetic formation of radicals can be similarly observed.

Effect of HA: HA acts as scavenger of oxidizing species, leading to a reduction in the degradation efficiency. As can be seen in Figure 4e, increasing the concentration of HA to 15 mg L^{-1} reduced k_{CT} from 0.039 min^{-1} to 0.014 min^{-1} (decreased by 64%), and the removal efficiency decreased from 68% to 23% after 30 min. This result can be explained by several mechanisms [16]: (1) HA competed with CT for the adsorption at the Pt cathode and BDD anode, thus, less CT was degraded at the surface of electrodes; (2) HA competed with sulfate ion on the BDD anode, leading to a reduction in the formation of $SO_4^{\bullet-}$ (Eq. (4)); (3) HA caused the scavenging effect toward •OH and $SO_4^{\bullet-}$ (Reactions (101) and (102), Table S2).

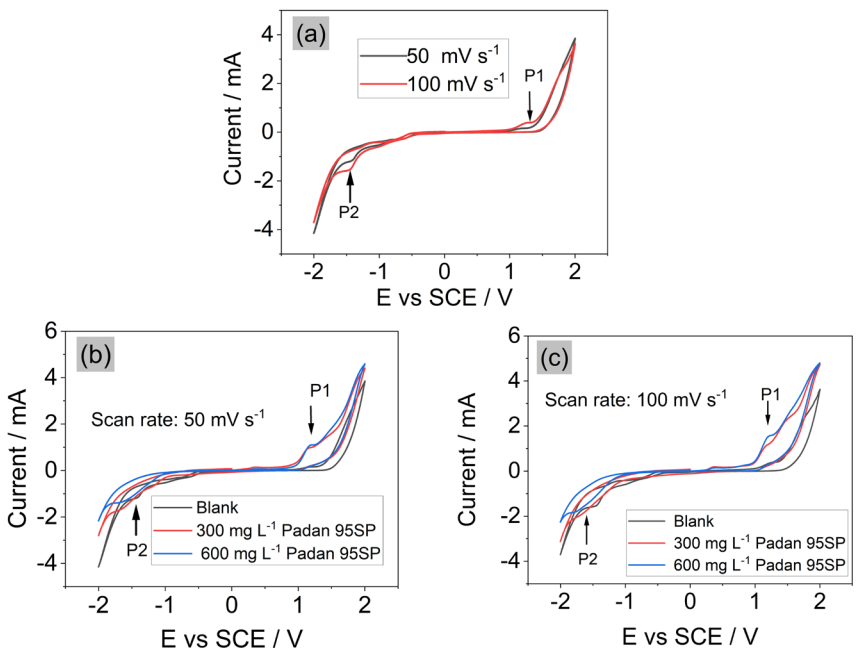

Figure 3. CVs of BDD in the presence of CT and Na_2SO_4. **a)** CVs of BDD in 300 mg L^{-1} CT at different scan rates. **b, c)** The comparison of CVs between blank solution and CT solution. 0.05 M Na_2SO_4 was used as supporting electrolyte.

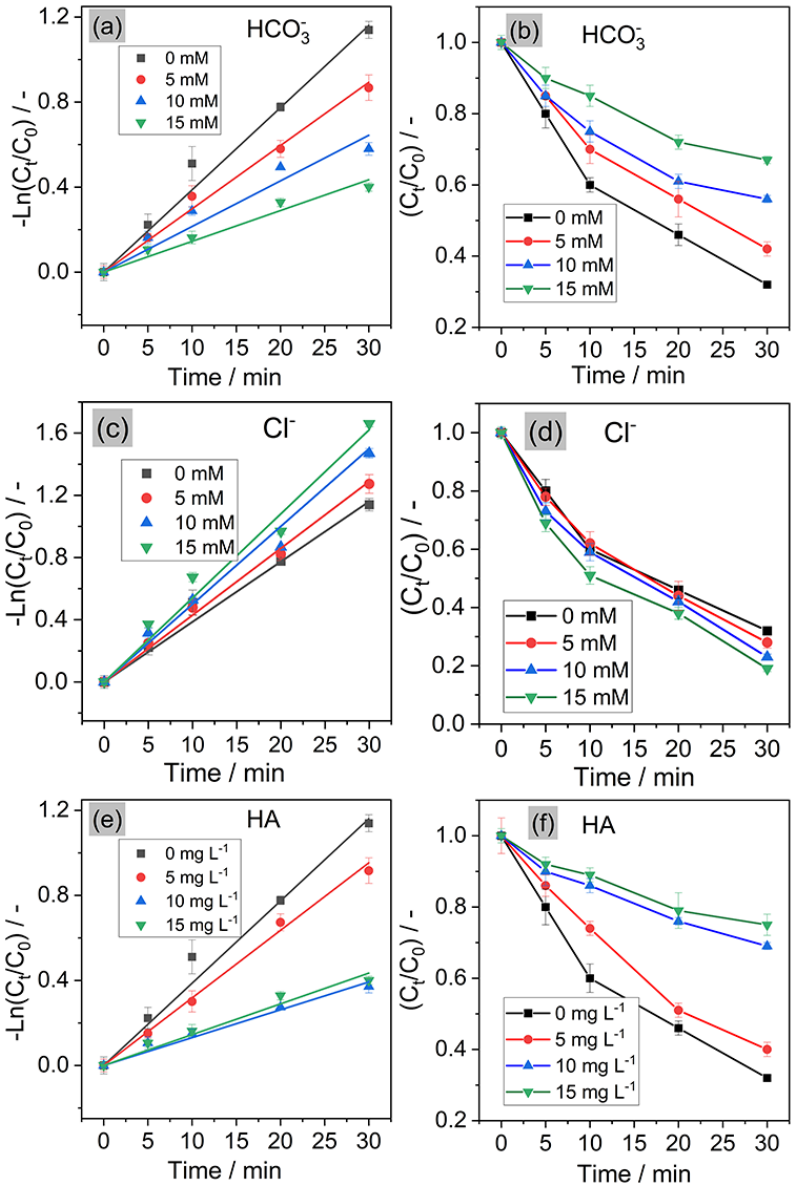

Figure 4. Effect of HCO_3^-, Cl^-, and HA on CT degradation in electrochemical process. (a, c, e) The first-order kinetics of CT in the presence of HCO_3^-, Cl^-, and HA, respectively. (b, d, f) Relative degradation of CT in the presence of HCO_3^-, Cl^-, and HA, respectively. Experimental conditions: pH = 3, current density j = 40 mA cm^{-2}, [CT] = 40 μM, [Na_2SO_4] = 0.05 M.

3.4. Determination of reactive species

Generally, •OH and $SO_4^{\bullet-}$ were found to be major radicals in EO process [22]. To determine the role of these radicals to CT degradation, TBA used as a scavenger for •OH ($k_{\bullet OH,TBA} = (3.8\text{-}7.6)\times10^8$ M^{-1} s^{-1}) [16]. The reaction between $SO_4^{\bullet-}$ and TBA can be ignored ($k_{SO_4^{\bullet-},TBA} = (4\text{-}9.1)\times10^5$ M^{-1} s^{-1}) [16]. MeOH was used as probe for •OH (9.7×40^8 $M^{-1}s^{-1}$) and $SO_4^{\bullet-}$ (1.0×10^7 $M^{-1}s^{-1}$). As seen in Figure 5a, k_{CT} decreased by 35% and 43% when adding 100 mM TBA and MeOH, respectively. CT removal efficiency decreased from 68% to 37% and to 29% after 30 min at 100 mM TBA and MeOH, respectively (Figure 5b). The significant decrease in k_{CT}, and k_{CT}(in TBA) > k_{CT}(in MeOH) suggested that •OH and $SO_4^{\bullet-}$ were the major radicals contributing to CT degradation. In addition, the other ROS ($O_2^{\bullet-}$, $O^{\bullet-}$, $HO_2^{\bullet}$, etc.) (Reactions (4-25), Table S2) could also form in the electrolysis process as the reaction chains in the solution. However, their role on CT degradation was assumed to be negligible due to their low concentration as suggested by [16].

3.5. The relative contribution of reactive species to CT degradation

In EO process, the oxidation of CT can be taken placed by several oxidizing factors as displayed in Eq. (5): •OH, $SO_4^{\bullet-}$, other ROS, and DET. To calculate the degradation of CT by DET, MeOH was used to eliminate the effect of ROS. Assuming that adding 10 M MeOH could scavenge all ROS (including •OH, $SO_4^{\bullet-}$) completely, then k_{DET} was calculated to be 0.006 min^{-1}, accounted for 15% of CT degradation (Figure 6). The change in k_{CT} with addition of scavengers can be seen in Figure 6. •OH and $SO_4^{\bullet-}$ could be generated by electrolysis alone at the surface of anode (Eqs. (2) and (4)) and/or from the reactions chains in solution (Reactions 1–29, Table S2). The relative contribution of •OH and $SO_4^{\bullet-}$ was calculated according to Eqs. (11) and (12) [22]. As a result, •OH and $SO_4^{\bullet-}$ accounted for 61.5% and 12.5%, respectively.

$$\eta_{\bullet OH} = \frac{k_{CT} - k_{TBA}}{k_{CT}} \times 100\% \tag{11}$$

$$\eta_{SO_4^{\bullet-}} = \frac{k_{MeOH} - k_{TBA}}{k_{CT}} \times 100\% \quad , \tag{12}$$

where k_{CT} represents the degradation rate constant of CT without addition of scavenger, min^{-1}; k_{TBA} represents the degradation rate constant of CT with addition of TBA (2.2 mM), min^{-1}; k_{MeOH} is the degradation rate constant with addition of MeOH (5 mM), min^{-1}.

Furthermore, to estimate the steady-state concentration of •OH and $SO_4^{\bullet-}$, NB and BA were used because NB can react with •OH ($k_{\bullet OH,NB} = 3.9\times10^9$ M^{-1} s^{-1}) and its reactivity toward $SO_4^{\bullet-}$ was negligible ($k_{SO_4^{\bullet-},NB} < 10^6$ M^{-1} s^{-1}) [23]. BA can react with both •OH and $SO_4^{\bullet-}$ ($k_{\bullet OH,BA} = 5.9\times10^9$ M^{-1} s^{-1}[24], ($k_{SO_4^{\bullet-},BA} = 1.2\times10^9 M^{-1}$ s^{-1}) [25]. Therefore, the degradation of NB and BA in EO process can be expressed as follows [26]:

$$k_{NB} = k_e + k_{\bullet OH,NB}[\bullet OH]_{ss} \tag{13}$$

$$k_{BA} = k_e + k_{\bullet OH,BA}[\bullet OH]_{ss} + k_{SO_4^{\bullet-},BA}[SO_4^{\bullet-}]_{ss} \, . \tag{14}$$

Assuming that the degradation of NB and BA by DET is negligible, the above reactions can be rewritten:

$$k_{NB} = k_{\bullet OH,NB}[\bullet OH]_{ss} \tag{15}$$

$$k_{BA} = k_{\bullet OH,BA}[\bullet OH]_{ss} + k_{SO_4^{\bullet-},BA}[SO_4^{\bullet-}]_{ss} \, , \tag{16}$$

where k_{NB}, k_{BA} (min^{-1}) represent the degradation of NB, BA in EO process (Experimental conditions were carried out similar to CT degradation: pH = 3, current density j = 40 mA cm^{-2}, [NB] = [BA] = 40 μM, [Na_2SO_4] = 50 mM, see Figure S3). By solving the reactions (15) and (16), $[\bullet OH]_{ss}$ and $[SO_4^{\bullet-}]_{ss}$ were estimated to be 3.2 × 10^{-13} M and 5.8 × 10^{-14} M, respectively.

The overview of the contribution of oxidants to CT degradation was listed in Table.

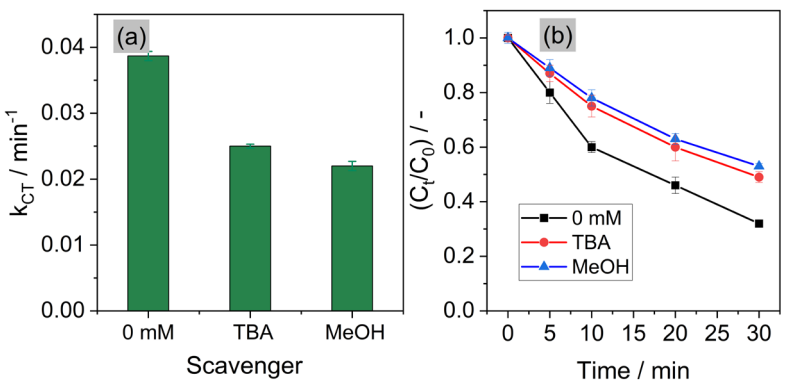

Figure 5. a) The first-order rate constant (k_{CT}) of CT degradation in the presence of TBA and MeOH; b) Relative degradation of CT in the presence of TBA and MeOH. Experimental conditions: pH = 3, current density j = 40 mA cm^{-2}, [CT] = 40 μM, [TBA] = [MeOH] = 100 mM, [Na_2SO_4] = 0.05 M.

3.6. Transformation and interaction mechanism of radicals

It is known that the degradation of organics was performed mainly by •OH radicals, so the mechanism of generating hydroxyl radicals on the anode surface is written as follows:

$$BDD + H_2O \rightarrow BDD(\bullet OH) + H^+ + e^- \quad (17)$$

$$BDD(\bullet OH) + CT \rightarrow CT\bullet + BDD + H^+ + e \quad (18)$$

$$BDD(\bullet OH) + CT\bullet \rightarrow BDD + \text{intermediates} + CO_2 + H_2O. \quad (19)$$

After losing electrons at the surface of BDD the H_2O molecules generate •OH radical (Eq. (17)). Hydroxyl radical is a strong oxidant, which can attack CT rapidly to generate radical CT•. As a low stable radical, CT• reacts with hydroxyl radical to further generate new intermediates and the end products (i.e. CO_2 and H_2O). Besides, the formation of $SO_4^{\bullet-}$ can take place through electron-transfer on the surface of BDD and/or from •OH. $SO_4^{\bullet-}$ then attacks CT to reproduce SO_4^{2-} and cationic radical $CT^{+\bullet}$, as described in Eqs. (20) and (21). $SO_4^{\bullet-}$ is considered as very active oxidant ($E^0 = 2.6$ V), can further destroy this organic radical to the end products, or generate smaller molecules.

$$HSO_4^- + \bullet OH \rightarrow SO_4^{\bullet-} + H_2O \quad (20)$$

$$SO_4^{\bullet-} + CT \rightarrow CT^{+\bullet} + H^+ + SO_4^{2-} \quad (21)$$

$$SO_4^{\bullet-} + CT^{+\bullet} \rightarrow SO_4^{2-} + CO_2 + H_2O \quad (22)$$

Additionally, some mechanisms involving with this radical may occur, as described in the reactions below:

$$SO_4^{\bullet-} + SO_4^{\bullet-} \rightarrow S_2O_8^{2-} \quad (23)$$

$$SO_4^{2-} \rightarrow SO_4^{\bullet-} + e^- \quad (24)$$

$$HSO_4^- \rightarrow SO_4^{\bullet-} + H^+ + e^- \quad (25)$$

$$SO_4^{\bullet-} + SO_4^{2-} \rightarrow S_2O_8^{2-} + e^- \quad (26)$$

$$SO_4^{\bullet-} + HSO_4^- \rightarrow S_2O_8^{2-} + H^+ + e^- . \quad (27)$$

In the presence of •OH, protonized HSO_4^- could be oxidized to form $SO_4^{\bullet-}$ (Eq. (20)), which can recombine (Eq. (23)) [27,28] or further react with sulfate and/or hydrosulfate ions to form persulfate $S_2O_8^{2-}$ (Eqs. (26) and (27)) [29,30], as confirmed by the work of F. Zhang et al. [14] using ESR spectrum. Furthermore, the evolution of O_2 takes place via a recombination of •OH as in Eq. (28) or from the hydrolysis of persulfate (Eq. (29)):

$$\bullet OH + \bullet OH \rightarrow O_2 + 2H^+ + 2e^- \quad (28)$$

$$S_2O_8^{2-} + H_2O \rightarrow HSO_4^- + 1/2O_2 . \quad (29)$$

It is worth nothing that the electrochemical degradation of organics is a complex of various mechanisms, in which the oxidizing radicals could be produced by different ways, involving in the degradation of organics as well as their none-used disappearance. Briefly, we can see the whole process of oxidizing CT in Figure 7. Additionally, the degradation pathway of CT in EO process can be found in our previous study [17].

4. Conclusion

The kinetic electrochemical degradation of CT (in Padan 95 SP) was investigated. The degradation of CT underwent two mechanisms: direct oxidation by electron transfer and indirect oxidation by reactive generated species. The removal efficiency of CT depended on the presence of water matrices: 15 mM Cl^- improved k_{CT} by 38%, while k_{CT} was reduced by 61.5% and 64% when adding 15 mM HCO_3^- and 15 mg L^{-1} HA, respectively. CT removal efficiency was reduced in the presence of MeOH and TBA, indicating that reactive species play an important role in CT degradation. The contribution of reactive oxidants was established: DFT accounted for 15%; •OH accounted for 61.5%; $SO_4^{\bullet-}$ accounted for 12.8%; ROS accounted for 8.5%. As a small part of study, the effect of applied current on CT degradation was investigated, indicating the O_2 evolution at higher current inhibited the CT removal. In addition, the possible transformation pathways of reactive species was suggested.

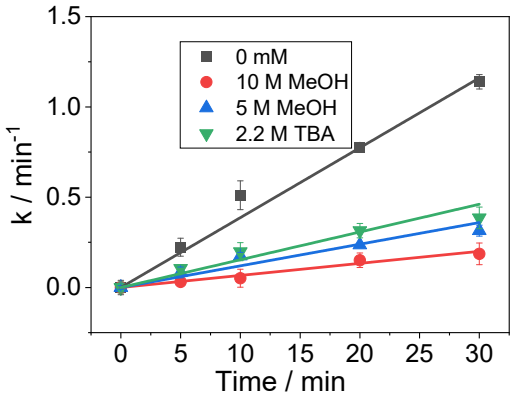

Figure 6. Reaction kinetics of CT in the presence of probes. Experimental conditions: pH = 3, current density j = 40 mA cm^{-2}, [CT] = 40 μM, [Na_2SO_4] = 0.05 M.

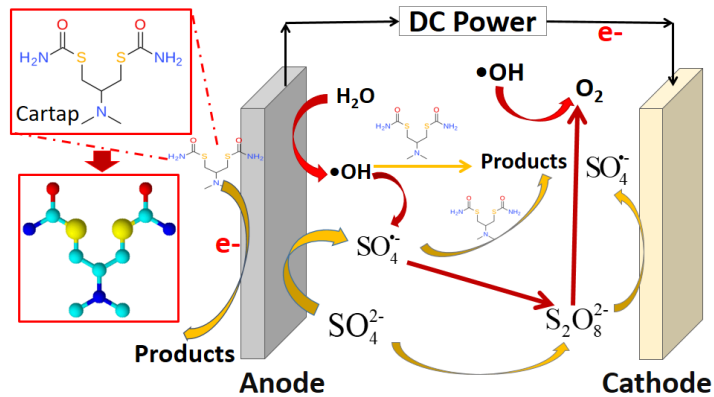

Figure 7. The electrochemical oxidation of CT and the transformation of radicals.

Table. The overview of the contribution of oxidants to CT degradation.

	DET	•OH	$SO_4^{\bullet-}$	other ROS
k_{CT} by oxidant, min^{-1}	0.007	0.024	0.005	0.003
Contribution, %	15	61.5	12.8	8.5
Concentration	-	3.2×10^{-13} M	5.8×10^{-14} M	(no detection)

Conflict of interest

The author declare no competing financial interest.

Acknowledgments

The author thanks Dr. Bui Dinh Nhi (Viet Tri University of Industry, Phu Tho, Viet Nam) for his SEM, XRD experimental support and helpful discussion, and Dr. Vo Thang Nguyen (University of Science and Education - The University of Danang) for her experimental support and helpful discussion.

References

1. Huy BT, Jung D, Kim Phuong NT, Lee YI. Enhanced photodegradation of 2,4-dichlorophenoxyacetic acid using a novel TiO2@MgFe2O4 core@shell structure. Chemosphere 2017; 184: 849-856. doi: 10.1016/j.chemosphere.2017.06.069
2. Li X, Zhou M, Pan Y, Xu L. Pre-magnetized Fe0/persulfate for notably enhanced degradation and dechlorination of 2,4-dichlorophenol. Chemical Engineering Journal 2017; 307: 1092-1104. doi: 10.1016/j.cej.2016.08.140
3. Brillas E, Sirés EI, Oturan MA. Electro-fenton process and related electrochemical technologies based on fenton's reaction chemistry. Chemical Reviews 2009; 109 (12): 6570-6631. doi: 10.1021/cr900136g
4. Coledam DAC, Aquino JM, Silva BF, Silva AJ, Rocha-Filho RC. Electrochemical mineralization of norfloxacin using distinct boron-doped diamond anodes in a filter-press reactor, with investigations of toxicity and oxidation by-products. Electrochimica Acta 2016; 213: 856-864. doi: 10.1016/j.electacta.2016.08.003
5. Zajda M, Aleksander KU. Wastewater treatment methods for effluents from the confectionery industry - an overview. Journal of Ecological Engineering 2019; 20 (9): 293-304. doi: 10.12911/22998993/112557
6. Dong H, Zeng G, Tang L, Fan C, Zhang C et al. An overview on limitations of TiO_2-based particles for photocatalytic degradation of organic pollutants and the corresponding countermeasures. Water Research 2015; 79: 128-146. doi: 10.1016/j.watres.2015.04.038
7. Jojoa-Sierra SD, Silva-Agredo J, Herrera-Calderon JE, Torres-Palma RA. Elimination of the antibiotic norfloxacin in municipal wastewater, urine and seawater by electrochemical oxidation on IrO2 anodes. Science of the Total Environment 2016; 575: 1228-1238. doi: 10.1016/j.scitotenv.2016.09.201
8. Panizza M, Cerisola G. direct and mediated anodic oxidation of organic pollutants. Chemical Reviews 2009; 109: 12, 6541-6569. doi: 10.1021/cr9001319
9. Hoang NT, Holze R. Degradation of pesticide Cartap in Padan 95SP by combined advanced oxidation and electro-Fenton process. Journal of solid state electrochemistry 2021; 25: 173-184. doi: 10.1007/s10008-020-04581-7
10. Hoang NT. Physical and electrochemical properties of Boron-Doped Diamond (BDD) electrode. Journal of Science and Technology 2020; 18 (6): 41-45.
11. Morao A, Lopes A, Pessoadeamorim M, Goncalves I. Degradation of mixtures of phenols using boron doped diamond electrodes for wastewater treatment. Electrochimica Acta 2004; 49 (9-10): 1587-1595. doi: 10.1016/S0013-4686(03)00966-6
12. Standards BI. Determination of cartap hydrochloride content (spectrophotometric method) copyrighted by Bureau of Indian Standards," IS 141591994.
13. Lee SJ, Caboni P, Tomizawa M, Casida JE. Cartap hydrolysis relative to its action at the insect nicotinic channel. Journal of Agricultural and Food Chemistry 2004; 52 (1): 95-98. doi: 10.1021/jf0306340
14. Zhang F, Sun Z, Cui J. Research on the mechanism and reaction conditions of electrochemical preparation of persulfate in a split-cell reactor using BDD anode. RSC Advances 2020; 10 (56): 33928-33936. doi: 10.1039/D0RA04669H
15. Wang HW, Bringans C, Hickey AJR, Windsor JA, Kilmartin P et al. Cyclic Voltammetry in Biological Samples: A Systematic Review of Methods and Techniques Applicable to Clinical Settings. Signals 2021; 2 (1): 138-158. doi: 10.3390/signals2010012
16. Liu Z, Ding H, Zhao C, Wang T, Wang P et al. Electrochemical activation of peroxymonosulfate with ACF cathode: Kinetics, influencing factors, mechanism, and application potential. Water Research 2019; 159: 111-121. doi: 10.1016/j.watres.2019.04.052
17. Hoang NT, Nguyen XC, Le PC, Juzsakova T, Chang SW et al. Electrochemical degradation of pesticide Padan 95SP by boron-doped diamond electrodes: The role of operating parameters. Journal of Environmental Chemical Engineering 2021; 9 (3): 105205. doi: 10.1016/j.jece.2021.105205
18. Lei Y, Lu J, Zhu M, Xie J, Peng S et al. Radical chemistry of diethyl phthalate oxidation via UV/peroxymonosulfate process: Roles of primary and secondary radicals. Chemical Engineering Journal 2020; 379: 122339. doi: 10.1016/j.cej.2019.122339
19. Lian L, Yao B, Hou S, Fang J, Yan S et al. Kinetic study of hydroxyl and sulfate radical-mediated oxidation of pharmaceuticals in wastewater effluents. Environmental Science & Technology 2017; 51 (5): 2954-2962. doi: 10.1021/acs.est.6b05536
20. W. Li, T. Jain, K. Ishida, H. Liu. A mechanistic understanding of the degradation of trace organic contaminants by UV/hydrogen peroxide, UV/persulfate and UV/free chlorine for water reuse. Environmental Science: Water Research & Technology 2017; 3 (1): 128-138. doi: 10.1039/C6EW00242K
21. Hoang NT, Nguyen VT, Tuan NDM, Manh TD, Le PC et al. Degradation of dyes by UV/Persulfate and comparison with other UV-based advanced oxidation processes: Kinetics and role of radicals. Chemosphere 2022; 298: 134197. doi: 10.1016/j.chemosphere.2022.134197
22. Cai J, Zhou M, Pan Y, Du X, Lu X. Extremely efficient electrochemical degradation of organic pollutants with co-generation of hydroxyl and sulfate radicals on Blue-TiO2 nanotubes anode. Applied Catalysis B: Environmental 2019; 257: 117902. doi: 10.1016/j.apcatb.2019.117902

23. Ji Y, Shi Y, Wang L, Lu J. Denitration and renitration processes in sulfate radical-mediated degradation of nitrobenzene. Chemical Engineering Journal 2017; 315: 591-597. doi: 10.1016/j.cej.2017.01.071

24. Buxton GV, Greenstock CL, Helman WP, Ross AB. Critical Review of rate constants for reactions of hydrated electrons, hydrogen atoms and hydroxyl radicals (·OH/·O − in Aqueous Solution. Journal of Physical and Chemical Reference Data 1988; 17 (2): 513-886. doi: 10.1063/1.555805

25. Neta P, Huie RE, Ross AB. Rate Constants for reactions of inorganic radicals in aqueous solution. Journal of Physical and Chemical Reference Data 1988; 17 (3): 1027-1284. doi: 10.1063/1.555808

26. Tan C, Jian X, Wu H, Sheng T, Sun TK et al. Kinetics degradation of phenacetin by solar activated persulfate system. Separation and Purification Technology 2021; 256: 117851. doi: 10.1016/j.seppur.2020.117851

27. Serrano K, Michaud PA, Comninellis C, Savall A. Electrochemical preparation of peroxodisulfuric acid using boron doped diamond thin film electrodes. Electrochimica Acta 2002; 48 (4): 431-436. doi: 10.1016/S0013-4686(02)00688-6

28. Ahna YY, Bae H, Kim HI, Kim SH, Kim JH et al. Surface-loaded metal nanoparticles for peroxymonosulfate activation: Efficiency and mechanism reconnaissance. Applied Catalysis B: Environmental 2019; 241: 561-569. doi: 10.1016/j.apcatb.2018.09.056

29. Davis J, Baygents JC, Farrell J. Understanding persulfate production at boron doped diamond film anodes. Electrochimica Acta 2014; 150: 68-74. doi: 10.1016/j.electacta.2014.10.104

30. Khamis D, Mahé E, Dardoize F, Devilliers D. Peroxodisulfate generation on boron-doped diamond microelectrodes array and detection by scanning electrochemical microscopy. Journal of Applied Electrochemistry 2010; 40 (10): 1829-1838. doi: 10.1007/s10800-010-0114-x

Supporting information Text S1: adsorptive possibility of BDD toward organic compounds

To check the change in concentration of CT and organic compounds in the presence of BDD without applied potential, different types of organic compounds were used. Those chosen compounds are dye compounds, which can be adsorbed high by some adsorbent (i.e. active carbon). However, there was no any reduction in concentration of CT and dye compounds (Figure S1), indicating that BDD is a nonadsorptive electrode.

Text S2: spectrum for Cartap detection

The absorbance spectrum of standard CT (in Padan 95SP) in the ranges of interested concentration were recorded in Figure S2 to establish the calibration curve for assessing the degradation of CT. It is also noted that the absorbance spectrum from CT decomposition during electrochemical process did not differ with the presence of other species (i.e. intermediates, electrolytes and pH). Condition for this measurement: 0.2 mL each trail was mixed well with 0.8 mL DTNB solution (1 g L^{-1} DTNB in methanol) and then with 4 mL buffer solution, as can be seen in detail elsewhere for preparing the sample for UV-Vis measurement [1,2].

Text S3: linear polarization curve

As a side reaction in electrochemical degradation of CT, the oxygen formation at BDD was assessed via linear sweep voltammetry (LSV). Thus, the linear polarization curves of BDD electrode was tested at two different scan rates of 50 and 100 mV s^{-1} in 0.05 M Na_2SO_4 electrolyte solution, as shown in Figure S4.

It is argued that the oxygen evolution reaction (OER) occurs since the current passing the electrode suddenly increases. Figure S4 shows that the higher OER (1.6 V) can be achieved at slower scan rate (50 mV s^{-1}), indicating the dependence of OER on scan rate. Additionally, the oxygen evolution overvoltage of both cases is pretty lower than that we expected from BDD. It should be kept in mind that the potential for oxygen evolution at anode is just a relative value and it might also differ under the experimental conditions. For example, Costa et al. [3] have pointed out that OER even occurred at the potential less than 2 V vs. SCE at 0.01 M H_2SO_4. They also showed a strong dependence of OER on the organic target, which contributes to a decrease in the potential of oxygen evolution when increasing its concentration. Similarly, O. Davila et al. figured out that the onset potentials for OER in electrolysis of BDD depends on the mixtures with dibenzothiophene (67 mg L^{-1} at scan rate: 10 mV s^{-1}) [4]. Some authors argued that the oxygen evolution rate decreased when adding organic compounds due to their competition with •OH [5,6]. In our condition, it is not an exceptional when we observed the low EOR. This might be due to the low concentration of supporting electrode (here: 0.05 M Na_2SO_4), dominating the oxygen evolution instead of oxidizing sulfate ions to other species. However, the anodic current is low within the potential interval from 1.50 to 2 V, indicating that not much oxygen was generated. The oxygen evolution at some BDD anodes are depicted in Table S1 below:

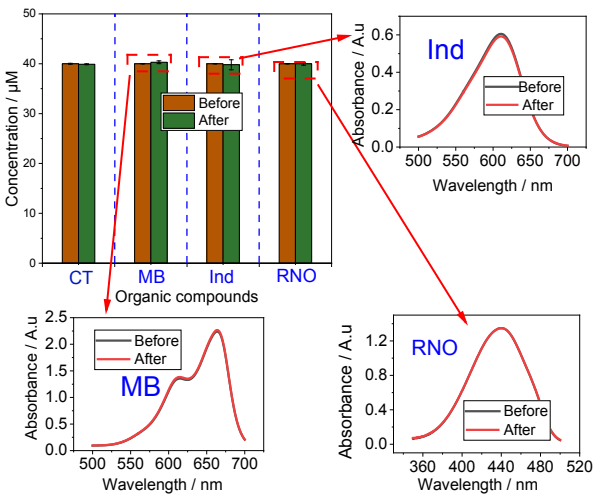

Figure S1. Concentration of organic compounds before and after immersed BDD electrode: CT (Cartap), MB (methylene blue), Ind (indigo carmine), RNO (P-nitrosodimethylaniline). The initial concentration of organic compounds was 40 μM, $V_{solution}$ = 100 mL.

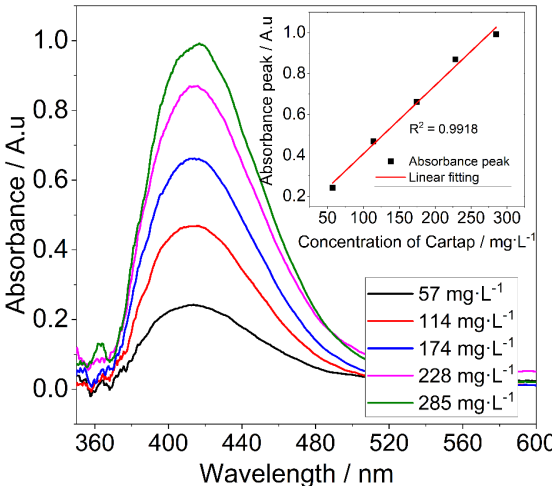

Figure S2. The intensity of absorbance spectra for calculating CT concentration in water. Insert: Calibration plot for calculating CT concentration based on data of Figure 2.

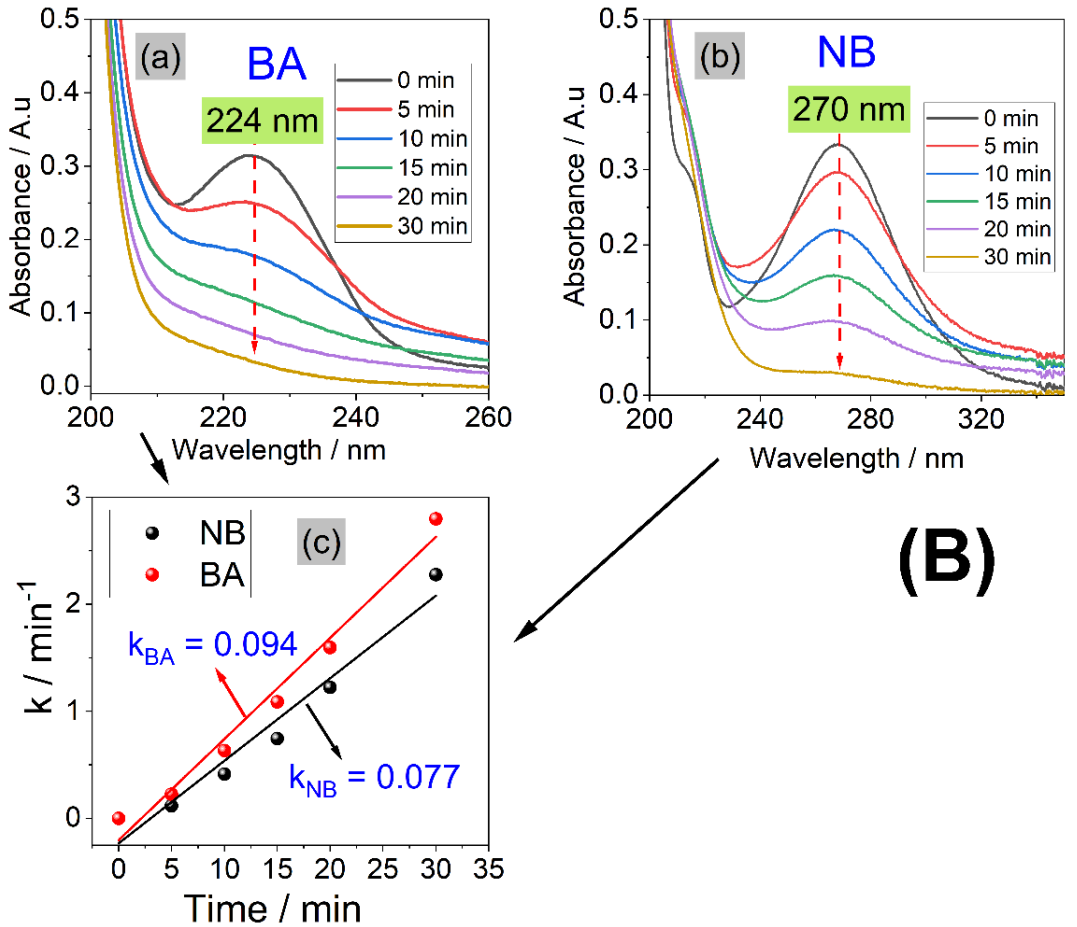

Figure S3. The kinetic degradation of NB and BA (by HPLC detection (A) and by UV-Vis detection (B)) to determine the concentration of •OH and SO_4•-. Experimental conditions: [NB] = [BA] = 40 μM, [Na_2SO_4] = 0.05 M, pH = 3, V = 250 mL, current density j = 40 mA cm^{-2}.

Text S4: effect of applied current density

The effect of the applied current density (j) on the CT degradation in the undivided cell is displayed in Figure S5.

As shown in Figure S5, the CT degradation rate increased at higher applied current density. More clearly, this result shows about 70% CT removed after 30 min at j = 40 mA cm^{-2}, meanwhile only 57% at j = 10 mA cm^{-2}. The result shows that this process fitted well the pseudo-first order kinetic, which is described by the Eq. (S1):

$$\ln(\frac{C_t}{C_0}) = -k_{CT}t\,, \tag{S1}$$

where C_t and C_0 are the concentration of CT at the interval time (t) and the beginning time, respectively. k_{CT} is the apparent rate constant of CT. We perform the degradation kinetic of CT in Figure S5b to determine the change in the k_{CT} versus current density. Obviously, k_{CT} increased from 0.022 min^{-1} to 0.039 min^{-1} (increased by 1.7-folds) when increasing the current density by 4 folds, suggesting that a production of·•OH radicals becomes inefficiently at higher current due to the competing reactions, here is oxygen evolution [10] (see Eq. (S2)). The fact can be demonstrated by mineralization current efficiency (MCE) in our previous paper [11]. This bubble gas can also deactivate surface of anode, thereby reducing the removal efficiency.

$$BDD(\bullet OH) \rightarrow BDD + \tfrac{1}{2}O_2 + H^+ + e^- \tag{S2}$$

Additionally, based on the calculation results for k_{CT} from Figures S5 and S6, and the suggestion of reference [12], we propose the relationship between the degradation rate constant k_{CT} and the applied current density j as the quadratic function, as shown in Figure S6.This function fits well our experimental results ranging from 10 mA cm^{-2} to 40 mA cm^{-2} with *R-square* of 0.978. Thus, we propose this relationship in Eq. (S3).

$$k_{CT} = 2\times10^{-5}j^2 + 5.8\times10^{-4}j + 0.019 \tag{S3}$$

Substitute the value k_{CT} from Eq. (1) into Eq. (S3), we obtain the kinetic reaction:

$$-\ln(\frac{C_t}{C_0}) = (2\times10^{-5}j^2 + 5.8\times10^{-4}j + 0.019)t\,, \tag{S4}$$

where C_t and C_0 (μM) are concentration of CT at time intervals t (min) and at the beginning, respectively. j is the current density (mA cm^{-1}).

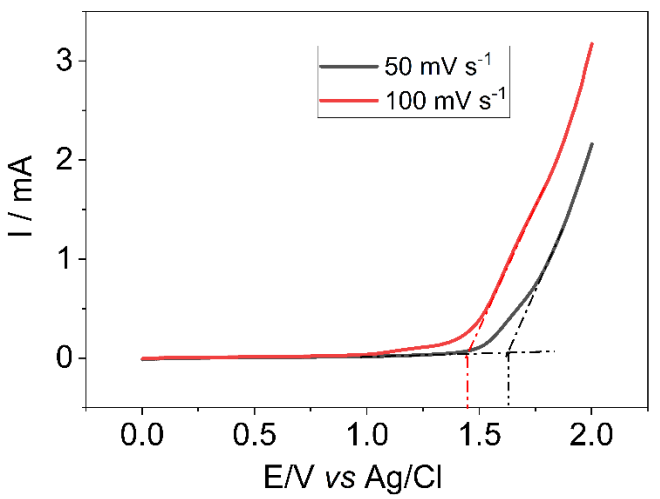

Figure S4. LSV of BDD in 0.05 M Na_2SO_4 at two scan rates. pH = 6.5 and at room temperature.

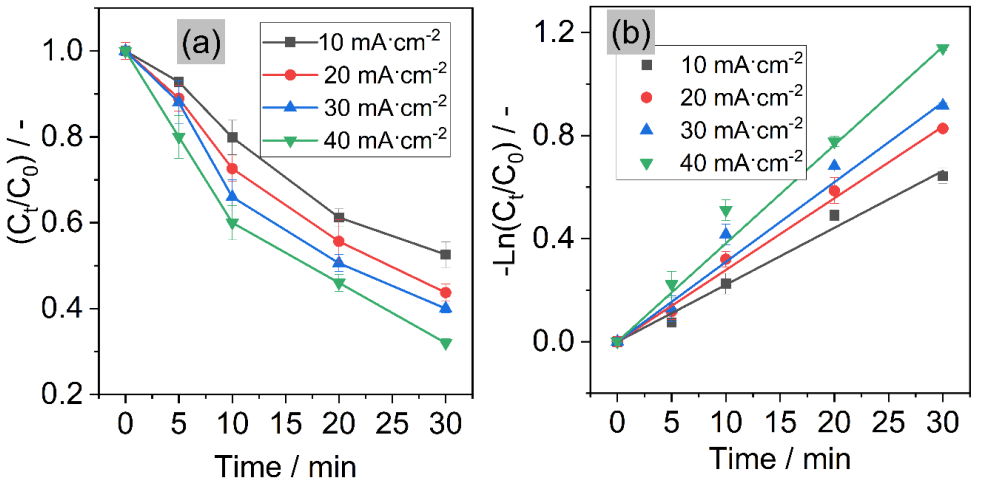

Figure S5. a) Effect of *j* on CT degradation as a function of time (*j* from 10 to 40 mA cm^{-2}). **b)** Effect of *j* on the apparent rate constant. Initial concentration of Padan 95SP (95% CT): 40 µM, supporting electrolyte: 0.05 M Na_2SO_4, pH = 3, BDD: working electrode.

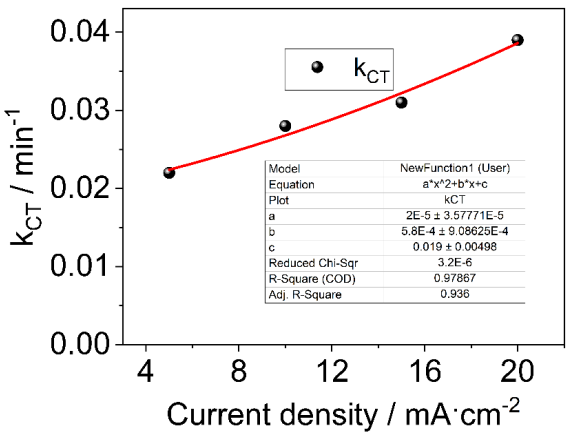

Figure S6. The plot of degradation rate constant versus current density.

Table S1. Potential for oxygen evolution on electrodes.

Anode	**E^0**	**Conditions**	**References**
Ti/BDD	2.7 V vs. SHE	0.5 M H_2SO_4	-
Mesh BDD	1.95 V vs. SCE	0.03 M Na_2SO_4, scan rate: 20 mV s^{-1}	[7]
BDD	1.5 V vs. SCE	1 M H_2SO_4, scan rate: 20 mV s^{-1}	[8]
BDD	0.9 V vs. SCE	0.25 M NaOH + 0.5 M Na_2SO_4, scan rate: 100 mV s^{-1}	[9]
BDD	2 V vs. SCE	0.5 M H_2SO_4, scan rate: 100 mV s^{-1}	[9]

Table S2. The kinetic model in electrochemical system.

No.	**Reaction**	k ($M^{-1}s^{-1}$) / s^{-1}	Reference
$HO_x^{\bullet}$ and $SO_x^{\bullet-}$ reactions			
1	$SO_4^{\bullet-} + SO_4^{\bullet-} \rightarrow S_2O^{82}$-	4.0×10^8 $M^{-1}s^{-1}$	[13]
2	$SO_4^{\bullet-} + OH^- \rightarrow {}^{\bullet}OH + SO_4^{2-}$	6.5×10^7 $M^{-1}s^{-1}$	[13]
3	${}^{\bullet}OH + {}^{\bullet}OH \rightarrow H_2O_2$	6.1×10^9 $M^{-1}s^{-1}$	[14]
4	${}^{\bullet}OH + OH^- \rightarrow O^{\bullet-} + H_2O$	1.2×10^{10} $M^{-1}s^{-1}$	[15]
5	${}^{\bullet}OH + SO_4^{\bullet-} \rightarrow HSO_5^-$	1.0×10^{10} $M^{-1}s^{-1}$	[13]
6	${}^{\bullet}OH + H_2O_2 \rightarrow HO_2^{\bullet} + H_2O$	2.7×10^7 $M^{-1}s^{-1}$	[13]
7	$HO_2^{\bullet} + HO_2^{\bullet} \rightarrow H_2O_2 + O_2$	8.3×10^5 $M^{-1}s^{-1}$	[14]
8	$HO_2^{\bullet} \rightarrow O_2^{\bullet-} + H^+$	7.0×10^5 s^{-1}	[16]
9	$H_2O_2 \rightarrow HO_2^- + H^+$	1.3×10^{-1} s^{-1}	[14]
10	$H_2O_2 + O_2^{\bullet-} \rightarrow {}^{\bullet}OH + OH^- + O_2$	1.3×10^{-1} $M^{-1}s^{-1}$	[17]
11	$H_2O_2 + O^{\bullet-} \rightarrow O_2^{\bullet-} + H_2O$	4.0×10^8 $M^{-1}s^{-1}$	[15]
12	$HO_2^- + H^+ \rightarrow H_2O_2$	5.0×10^{10} $M^{-1}s^{-1}$	[14]
13	$H_2O \rightarrow H^+ + OH^-$	1.0×10^{-3} $M^{-1}s^{-1}$	[14]
14	$H^+ + OH^- \rightarrow H_2O$	1.0×10^{11} $M^{-1}s^{-1}$	[14]
15	$O_2^{\bullet-} + H^+ \rightarrow HO_2^{\bullet}$	5.0×10^{10} $M^{-1}s^{-1}$	[16]
16	$HO_2^{\bullet} + O_2^{\bullet-} \rightarrow HO_2^- + O_2$	9.7×10^7 $M^{-1}s^{-1}$	[16]
17	${}^{\bullet}OH + HO_2^{\bullet} \rightarrow H_2O + O_2$	7.1×10^9 $M^{-1}s^{-1}$	[16]
18	${}^{\bullet}OH + O_2^{\bullet-} \rightarrow OH^- + O_2$	1.0×10^{10} $M^{-1}s^{-1}$	[16]
19	${}^{\bullet}OH + O^{\bullet-} \rightarrow HO_2^-$	1.0×10^{10} $M^{-1}s^{-1}$	[15]
20	${}^{\bullet}OH + HO_2^- \rightarrow H_2O + O_2^{\bullet-}$	7.5×10^9 $M^{-1}s^{-1}$	[13]
21	${}^{\bullet}OH + HSO_5^- \rightarrow SO_5^{\bullet-} + H_2O$	1.7×10^7 $M^{-1}s^{-1}$	[13]
22	$SO_4^{\bullet-} + HSO_5^- \rightarrow SO_5^{\bullet-} + HSO^4$-	1.0×10^5 $M^{-1}s^{-1}$	[18]
23	$SO_4^{\bullet-} + S_2O_8^{2-} \rightarrow SO_4^{2-} + S_2O^{8\bullet}$-	6.1×10^5 $M^{-1}s^{-1}$	[18]
24	$SO_4^{\bullet-} + H_2O_2 \rightarrow HO_2^{\bullet} + HSO^4$-	1.2×10^7 $M^{-1}s^{-1}$	[13]
25	$SO_4^{\bullet-} + H_2O_2 \rightarrow HO_2^{\bullet} + H^+ + SO_4^{2-}$	1.2×10^7 $M^{-1}s^{-1}$	[19]
26	$HSO_4^- + {}^{\bullet}OH \rightarrow SO_4^{\bullet-} + H_2O$	6.9×10^5 $M^{-1}s^{-1}$	[13]
27	$2SO_5^{\bullet-} \rightarrow 2SO_4^{\bullet-} + O_2$	1.0×10^8 s^{-1}	[13]
28	$2SO_5^{\bullet-} \rightarrow S_2O_8^{2-} + O_2$	2.2×10^8 s^{-1}	[20]
29	$HSO_4^- \rightarrow SO_4^{2-} + H^+$	1.2×10^{-2} $M^{-1}s^{-1}$	[13]
CT reactions			
	Primary radicals with CT		
30	${}^{\bullet}OH + CT \rightarrow pro$	10^9–10^{10} $M^{-1}s^{-1}$	Estimated
31	$SO_4^{\bullet-} + CT \rightarrow pro + SO_4^{2-}$	10^9–10^{10} $M^{-1}s^{-1}$	Estimated
	Secondary radicals with CT		
32	$Cl^{\bullet} + CT \rightarrow pro$	10^9–10^{10} $M^{-1}s^{-1}$	Estimated
33	$Cl_2^{\bullet-} + CT \rightarrow pro$	-	-
34	$CO_3^{\bullet-} + CT \rightarrow pro$	10^6–10^7 $M^{-1}s^{-1}$	Estimated
Chloride reactions			
35	$SO_4^{\bullet-} + Cl^- \rightarrow SO_4^{2-} + Cl^{\bullet}$	4.7×10^8 $M^{-1}s^{-1}$	[18]
36	$SO_4^{2-} + Cl^{\bullet} \rightarrow SO_4^{\bullet-} + Cl^-$	2.5×10^8 $M^{-1}s^{-1}$	[18]

Table S2 (Continued).

37	$Cl^- + {}^\bullet OH \rightarrow ClOH^{\bullet-}$	4.3×10^9 $M^{-1}s^{-1}$	[14]
38	$ClOH^{\bullet-} + Cl^- \rightarrow Cl_2^{\bullet-} + OH^-$	1.0×10^5 $M^{-1}s^{-1}$	[14]
39	$ClOH^{\bullet-} \rightarrow Cl^- + {}^\bullet OH$	6.1×10^9 $M^{-1}s^{-1}$	[14]
40	$ClOH^{\bullet-} + H^+ \rightarrow Cl^\bullet + H_2O$	2.1×10^{10} $M^{-1}s^{-1}$	[14]
41	$Cl^- + Cl^\bullet \rightarrow Cl_2^{\bullet-}$	6.5×10^9 $M^{-1}s^{-1}$	[14]
42	$Cl^\bullet + Cl^\bullet \rightarrow Cl_2$	1.0×10^8 $M^{-1}s^{-1}$	[14]
43	$Cl^\bullet + H_2O \rightarrow HClOH$	2.5×10^5 $M^{-1}s^{-1}$	[14]
44	$Cl^\bullet + H_2O \rightarrow ClOH^{\bullet-} + H^+$	1.6×10^5 $M^{-1}s^{-1}$	[14]
45	$Cl_2^{\bullet-} + OH^- \rightarrow ClOH^{\bullet-} + Cl^-$	4.5×10^7 $M^{-1}s^{-1}$	[14]
46	$Cl^\bullet + OH^- \rightarrow ClOH^{\bullet-}$	1.8×10^{10} $M^{-1}s^{-1}$	[14]
47	$H^+ + Cl^- \rightarrow HCl$	5.0×10^{10} $M^{-1}s^{-1}$	[14]
48	$HCl \rightarrow H^+ + Cl^-$	8.6×10^{16} $M^{-1}s^{-1}$	[14]
49	$Cl^- + Cl_2 \rightarrow Cl_3^-$	2.0×10^4 $M^{-1}s^{-1}$	[14]
50	$Cl_2^{\bullet-} \rightarrow Cl^\bullet + Cl^-$	1.1×10^5 $M^{-1}s^{-1}$	[14]
51	$Cl_2^{\bullet-} + Cl_2^{\bullet-} \rightarrow Cl_2 + 2Cl^-$	8.3×10^8 $M^{-1}s^{-1}$	[14]
52	$Cl^\bullet + H_2O_2 \rightarrow HCl + HO_2^\bullet$	4.0×10^9 $M^{-1}s^{-1}$	[14]
53	$Cl_2^{\bullet-} + H_2O_2 \rightarrow 2Cl^- + HO_2^\bullet + H^+$	1.4×10^5 $M^{-1}s^{-1}$	[16]
54	$Cl_2^{\bullet-} + H_2O \rightarrow HClOH + Cl^-$	1.3×10^3 $M^{-1}s^{-1}$	[14]
55	$Cl_2^{\bullet-} + {}^\bullet OH \rightarrow HOCl + Cl^-$	1.0×10^9 $M^{-1}s^{-1}$	[14]
56	$Cl^- + HOCl \rightarrow Cl_2OH^-$	1.5×10^4 $M^{-1}s^{-1}$	[16]
57	$Cl_2^{\bullet-} + O_2^{\bullet-} \rightarrow 2Cl^- + O_2$	1.0×10^9 $M^{-1}s^{-1}$	[14]
58	$HOCl \rightarrow H^+ + ClO^-$	1.6×10^3 s^{-1}	[14]
59	$H^+ + ClO^- \rightarrow HOCl$	5.0×10^{10} $M^{-1}s^{-1}$	[14]
60	$HClOH \rightarrow ClOH^{\bullet-} + H^+$	1.0×10^8 s^{-1}	[14]
61	$HClOH \rightarrow Cl^\bullet + H_2O$	1.0×10^2 s^{-1}	[14]
62	$HClOH + Cl^- \rightarrow Cl_2^{\bullet-} + H_2O$	5.0×10^9 $M^{-1}s^{-1}$	[14]
63	$Cl_3^- + HO_2^\bullet \rightarrow Cl_2^{\bullet-} + HCl + O_2$	1.0×10^9 $M^{-1}s^{-1}$	[14]
64	$Cl_3^- + O_2^{\bullet-} \rightarrow Cl_2^{\bullet-} + Cl^- + O_2$	3.8×10^9 $M^{-1}s^{-1}$	[14]
65	$Cl_3^- \rightarrow Cl_2 + Cl^-$	1.1×10^5 s^{-1}	[14]
66	$Cl_2 + O_2^{\bullet-} \rightarrow Cl_2^{\bullet-} + O_2$	1.0×10^9 $M^{-1}s^{-1}$	[14]
67	$Cl_2 + HO_2^\bullet \rightarrow Cl_2^{\bullet-} + H^+ + O_2$	1.0×10^9 $M^{-1}s^{-1}$	[13]
68	$Cl_2 + H_2O \rightarrow Cl_2OH^- + H^+$	1.5×10^1 $M^{-1}s^{-1}$	[14]
69	$Cl_2 + H_2O \rightarrow HOCl + H^+ + Cl^-$	1.0×10^{-3} $M^{-1}s^{-1}$	[14]
70	$Cl_2 + H_2O_2 \rightarrow 2HCl + O_2$	1.3×10^4 $M^{-1}s^{-1}$	[14]
71	$Cl_2OH^- + H^+ \rightarrow Cl_2 + H_2O$	2.0×10^{10} $M^{-1}s^{-1}$	[14]
72	$Cl_2OH^- \rightarrow HOCl + Cl^-$	6.1×10^9 s^{-1}	[14]
73	$HOCl + {}^\bullet OH \rightarrow ClO^\bullet + H_2O$	2.0×10^9 $M^{-1}s^{-1}$	[13]
74	$HOCl + O_2^{\bullet-} \rightarrow Cl^\bullet + OH^- + O_2$	7.5×10^6 $M^{-1}s^{-1}$	[13]
75	$HOCl + HO_2^\bullet \rightarrow Cl^\bullet + H_2O + O_2$	7.5×10^6 $M^{-1}s^{-1}$	[14]
76	$HOCl + H_2O_2 \rightarrow HCl + H_2O + O_2$	1.1×10^4 $M^{-1}s^{-1}$	[14]
77	$ClO^- + {}^\bullet OH \rightarrow ClO^\bullet + OH^-$	8.8×10^9 $M^{-1}s^{-1}$	[14]
78	$ClO^- + H_2O_2 \rightarrow Cl^- + H_2O + O_2$	1.7×10^5 $M^{-1}s^{-1}$	[14]
79	$ClO^- + O_2^{\bullet-} + H_2O \rightarrow Cl^\bullet + 2OH^- + O_2$	2.0×10^8 $M^{-1}s^{-1}$	[14]
80	$Cl_2^{\bullet-} + HO_2^{\bullet-} \rightarrow 2Cl^- + H^+ + O_2$	3.0×10^9 $M^{-1}s^{-1}$	[14]

Table S2 (Continued).

CO_3^{2-} reactions			
81	$CO_3^{2-} + H^+ \rightarrow HCO_3^-$	5×10^{10} $M^{-1}s^{-1}$	[21]
82	$CO_3^{2-} + {}^{\bullet}OH \rightarrow CO_3^{\bullet-} + OH^-$	3.9×10^8 $M^{-1}s^{-1}$	[15]
83	$CO_3^{2-} + SO_4^{\bullet-} \rightarrow CO_3^{\bullet-} + SO_4^{2-}$	6.1×10^6 $M^{-1}s^{-1}$	[22]
84	$CO_3^{2-} + Cl^{\bullet} \rightarrow CO_3^{\bullet-} + Cl^-$	5×10^8 $M^{-1}s^{-1}$	[23]
85	$CO_3^{2-} + Cl_2^{\bullet-} \rightarrow CO_3^{\bullet-} + 2Cl^-$	1.6×10^8 $M^{-1}s^{-1}$	[21]
86	$CO_3^{2-} + ClO^{\bullet} \rightarrow CO_3^{\bullet-} + ClO^-$	6×10^2 $M^{-1}s^{-1}$	[24]
87	$HCO_3^- + H^+ \rightarrow H_2CO_3$	5×10^{10} $M^{-1}s^{-1}$	[25]
88	$HCO_3^- + {}^{\bullet}OH \rightarrow CO_3^{\bullet-} + H_2O$	8.6×10^6 $M^{-1}s^{-1}$	[15]
89	$HCO_3^- + Cl^{\bullet} \rightarrow CO_3^{\bullet-} + HCl$	2.2×10^6 $M^{-1}s^{-1}$	[23]
90	$HCO_3^- + Cl_2^{\bullet-} \rightarrow 2Cl^- + H^+ + CO_3^{\bullet-}$	8.0×10^7 $M^{-1}s^{-1}$	[21]
91	$HCO_3^- + SO_4^{\bullet-} \rightarrow CO_3^{\bullet-} + SO_4^{2-} + H^+$	9.1×10^6 $M^{-1}s^{-1}$	[26]
92	$H_2CO_3 + {}^{\bullet}OH \rightarrow CO_3^{\bullet-} + H_2O + H^+$	1.0×10^6 $M^{-1}s^{-1}$	[14]
93	$H_2CO_3 \rightarrow HCO_3^- + H^+$	2.5×10^4 $M^{-1}s^{-1}$	[27]
94	$CO_3^{\bullet-} + H_2O_2 \rightarrow HCO_3^- + HO_2^{\bullet}$	4.3×10^5 $M^{-1}s^{-1}$	[28]
95	$CO_3^{\bullet-} + HO_2^- \rightarrow CO_3^{2-} + HO_2^{\bullet}$	3×10^7 $M^{-1}s^{-1}$	[28]
96	$CO_3^{\bullet-} + {}^{\bullet}OH \rightarrow$ pro	3×10^9 $M^{-1}s^{-1}$	[29]
97	$CO_3^{\bullet-} + CO_3^{\bullet-} \rightarrow$ pro	3×10^7 $M^{-1}s^{-1}$	[29]
98	$CO_3^{\bullet-} + O_2^{\bullet-} \rightarrow CO_3^{2-} + O_2$	6×10^8 $M^{-1}s^{-1}$	[29]
99	$CO_3^{\bullet-} + 2Br^- \rightarrow CO_3^{2-} + Br_2^-$	3.4×10^4 $M^{-1}s^{-1}$	[24]
100	$CO_3^{\bullet-} + ClO^- \rightarrow CO_3^{2-} + ClO^{\bullet}$	5.1×10^5 $M^{-1}s^{-1}$	[30]
NOM reactions			
101	NOM + $HO^{\bullet} \rightarrow$ X	2.5×10^4 $(mg\ L^{-1})^{-1}\ s^{-1}$	[31]
102	NOM + $SO_4^{\bullet-} \rightarrow$ X	5.1×10^3 $(mg\ L^{-1})^{-1}\ s^{-1}$	[25]

References

1. Standards BT. Determination of cartap hydrochloride content (spectrophotometric method) copyrighted by Bureau of Indian Standards. IS 141591994.
2. Lee SJ, Caboni P, Tomizawa M, Casida JE. Cartap Hydrolysis Relative to Its Action at the Insect Nicotinic Channel. Journal of Agricultural and Food Chemistry 2004; 52 (1): 95-98. doi: 10.1021/jf0306340.
3. Costa TD, Santos J, Silva D, Martinez-Huitle C. BDD-Electrolysis of Oxalic Acid in Diluted Acidic Solutions. Journal of the Brazilian Chemical Society 2019; 30 (7): 1541-1547. doi: 10.21577/0103-5053.20190051.
4. Dávila OO, Bergeron LL, Gutiérrez PR, Jiménez MMD, Sirés I, Brillas E, Navarro AFR, Arandes JB, Llopis JVS. Electrochemical oxidation of dibenzothiophene compounds on BDD electrode in acetonitrile-water medium. Journal of Electroanalytical Chemistry 2019; 847: 113172. doi: 10.1016/j.jelechem.2019.05.054.
5. Kisacik I, Stefanova A, Ernst S, Baltruschat H. Oxidation of carbon monoxide, hydrogen peroxide and water at a boron doped diamond electrode: the competition for hydroxyl radicals," Physical Chemistry Chemical Physics 2013; 15 (13): 4616. doi: 10.1039/c3cp44643c.
6. Mitroka S, Zimmeck S, Troya D, Tanko JM. How Solvent Modulates Hydroxyl Radical Reactivity in Hydrogen Atom Abstractions. Journal of the American Chemical Society 2010; 132 (9): 2907–2913. doi: 10.1021/ja903856t.
7. Pupo MM, Oliva JMA, Barrios EKI, Salazar-Banda GR, Radjenovic J. Characterization and comparison of Ti/TiO2-NT/SnO2–SbBi, Ti/SnO2–SbBi and BDD anode for the removal of persistent iodinated contrast media (ICM). Chemosphere 2020; 253: 126701. doi: 10.1016/j.chemosphere.2020.126701.
8. Pacheco-Álvarez MO. Improvement of the Degradation of Methyl Orange Using a TiO2/BDD Composite Electrode to Promote Electrochemical and Photoelectro-Oxidation Processes. International Journal of Electrochemical Science 2018; 13: 11549–11567. doi: 10.20964/2018.12.70.
9. Martínez-Huitle CA, Ferro S, Reyna S, Cerro-López M, De Battisti A et al. Electrochemical oxidation of oxalic acid in the presence of halides at boron doped diamond electrode," Journal of the Brazilian Chemical Society 2008; 19 (1): 150–156. doi: 10.1590/S0103-50532008000100021.
10. Yavuz Y, Shahbazi R. Anodic oxidation of Reactive Black 5 dye using boron doped diamond anodes in a bipolar trickle tower reactor. Separation and Purification Technology 2012; 85: 130–136. doi: 10.1016/j.seppur.2011.10.001.
11. Hoang NT, Nguyen XC, Le PC, Juzsakova T, Chang SW et al. Electrochemical degradation of pesticide Padan 95SP by boron-doped diamond electrodes: The role of operating parameters. Journal of Environmental Chemical Engineering 2021; 9 (3): 105205. doi: 10.1016/j.jece.2021.105205.
12. Panizza M, Kapalka A, Comninellis C. Oxidation of organic pollutants on BDD anodes using modulated current electrolysis. Electrochimica Acta 2008; 53 (5): 2289–2295. doi: 10.1016/j.electacta.2007.09.044.
13. Guan YH, Ma J, Li XC, Fang JY, Chen LW. Influence of pH on the Formation of Sulfate and Hydroxyl Radicals in the UV/Peroxymonosulfate System. Environmental Science & Technology 2011; 45 (21): 9308–9314. doi: 10.1021/es2017363.
14. Grebel JE, Pignatello JJ, Mitch WA. Effect of Halide Ions and Carbonates on Organic Contaminant Degradation by Hydroxyl Radical-Based Advanced Oxidation Processes in Saline Waters," Environmental Science & Technology 2010; 44 (17): 6822–6828. doi: 10.1021/es1010225.
15. Buxton GV, Greenstock CL, Helman WP, Ross AB. Critical Review of rate constants for reactions of hydrated electrons, hydrogen atoms and hydroxyl radicals (·OH/·O − in Aqueous Solution. Journal of Physical and Chemical Reference Data 1988; 17 (2): 513-886. doi: 10.1063/1.555805.
16. Liang C, Wang ZS, Mohanty N. Influences of carbonate and chloride ions on persulfate oxidation of trichloroethylene at 20 °C. Science of The Total Environment 2006; 370 (2–3): 271–277. doi: 10.1016/j.scitotenv.2006.08.028.
17. Weinstein J, Bielski BHJ. Kinetics of the interaction of perhydroxyl and superoxide radicals with hydrogen peroxide. The Haber-Weiss reaction. Journal of the American Chemical Society 1979; 101 (1): 58–62. doi: 10.1021/ja00495a010.
18. Yu XY, Bao ZC, Barker JR. Free Radical Reactions Involving Cl•, Cl2•- , and SO4•- in the 248 nm Photolysis of Aqueous Solutions Containing S2O82- and Cl-. The Journal of Physical Chemistry A 2004; 108 (2): 295–308. doi: 10.1021/jp036211i.
19. Maruthamuthu P, Neta P. Radiolytic chain decomposition of peroxomonophosphoric and peroxomonosulfuric acids. The Journal of Physical Chemistry 1977; 81 (10): 937–940. doi: 10.1021/j100525a001.
20. Das TN. Reactivity and Role of SO5•- Radical in Aqueous Medium Chain Oxidation of Sulfite to Sulfate and Atmospheric Sulfuric Acid Generation. The Journal of Physical Chemistry A 2001; 105 (40): 9142–9155. doi: 10.1021/jp011255h.

21. Matthew BM, Anastasio C. A chemical probe technique for the determination of reactive halogen species in aqueous solution: Part 1 – bromide solutions. Atmospheric Chemistry and Physics 2006: 6 (9): 2423–2437. doi: 10.5194/acp-6-2423-2006.

22. Zuo Z, Cai Z, Katsumura Y, Chitose N, Muroya Y. Reinvestigation of the acid–base equilibrium of the (bi)carbonate radical and pH dependence of its reactivity with inorganic reactants. Radiation Physics and Chemistry 1999; 55 (1): 15–23. doi: 10.1016/S0969-806X(98)00308-9.

23. Mertens R, Sonntag CV. Photolysis (λ = 354 nm of tetrachloroethene in aqueous solutions. Journal of Photochemistry and Photobiology A: Chemistry 1995; 85 (1-2): 1–9. doi: 10.1016/1010-6030(94)03903-8.

24. Huie RE, Clifton CL, Neta P. Electron transfer reaction rates and equilibria of the carbonate and sulfate radical anions. Int. J. Radiat. Appl. Instrumentation. Part C. Radiation Physics and Chemistry 1991; 38 (5): 477–481. doi: 10.1016/1359-0197(91)90065-A.

25. Yang Y, Pignatello JJ, Ma J, Mitch WA. Comparison of Halide Impacts on the Efficiency of Contaminant Degradation by Sulfate and Hydroxyl Radical-Based Advanced Oxidation Processes (AOPs). Environmental Science & Technology 2014; 48 (4): 2344–2351. doi: 10.1021/es404118q.

26. Dogliotti L, Hayon E. Flash photolysis of per[oxydi]sulfate ions in aqueous solutions. The sulfate and ozonide radical anions. The Journal of Physical Chemistry 1967; 71 (8): 2511–2516. doi: 10.1021/j100867a019.

27. Sunka P, Babický V, Clupek M, Lukes P, Simek M et al. Generation of chemically active species by electrical discharges in water. Plasma Sources Science and Technology 1999; 8: 258–258. Doi: 10.1088/0963-0252/8/2/006

28. Draganić ZD, Negrón-Mendoza A, Sehested K, Vujošević SI, Navarro-Gonzáles R et al. Radiolysis of aqueous solutions of ammonium bicarbonate over a large dose range. International Journal of Radiation Applications and Instrumentation. Part C. Radiation Physics and Chemistry 1991; 38 (3): 317–321. doi: 10.1016/1359-0197(91)90100-G.

29. Crittenden JC, Hu S, Hand DW, Green SA. A kinetic model for H2O2/UV process in a completely mixed batch reactor. Water Research 1999; 33 (10): 2315–2328. doi: 10.1016/S0043-1354(98)00448-5.

30. Alfassi ZB, Huie RE, Mosseri S, Neta P. Kinetics of one-electron oxidation by the ClO radical," Int. J. Radiat. Appl. Instrumentation. Part C. Radiation Physics and Chemistry 1988; 32 (1): 85–88. doi: 10.1016/1359-0197(88)90018-5.

31. Wua Z, Fang J, Xiang Y, Shang C, Li X et al. Roles of reactive chlorine species in trimethoprim degradation in the UV/chlorine process: Kinetics and transformation pathways. Water Research 2016; 104: 272–282. doi: 10.1016/j.watres.2016.08.011.

32. Coledam DAC, Aquino JM, Silva BF, Silva AJ, Rocha-Filho RC. Electrochemical mineralization of norfloxacin using distinct boron-doped diamond anodes in a filter-press reactor, with investigations of toxicity and oxidation by-products. Electrochimica Acta 2016; 213: 856-864. doi: 10.1016/j.electacta.2016.08.003

33. Zajda M, Aleksander KU. Wastewater treatment methods for effluents from the confectionery industry - an overview. Journal of Ecological Engineering 2019; 20 (9): 293-304. doi: 10.12911/22998993/112557

34. Dong H, Zeng G, Tang L, Fan C, Zhang C et al. An overview on limitations of TiO_2-based particles for photocatalytic degradation of organic pollutants and the corresponding countermeasures. Water Research 2015; 79: 128-146. doi: 10.1016/j.watres.2015.04.038

35. Jojoa-Sierra SD, Silva-Agredo J, Herrera-Calderon JE, Torres-Palma RA. Elimination of the antibiotic norfloxacin in municipal wastewater, urine and seawater by electrochemical oxidation on IrO2 anodes. Science of the Total Environment 2016; 575: 1228-1238. doi: 10.1016/j.scitotenv.2016.09.201

36. Panizza M, Cerisola G. direct and mediated anodic oxidation of organic pollutants. Chemical Reviews 2009; 109: 12, 6541-6569. doi: 10.1021/cr9001319

37. Hoang NT, Holze R. Degradation of pesticide Cartap in Padan 95SP by combined advanced oxidation and electro-Fenton process. Journal of solid state electrochemistry 2021; 25: 173-184. doi: 10.1007/s10008-020-04581-7

38. Hoang NT. Physical and electrochemical properties of Boron-Doped Diamond (BDD) electrode. Journal of Science and Technology 2020; 18 (6): 41-45.

39. Morao A, Lopes A, Pessoadeamorim M, Goncalves I. Degradation of mixtures of phenols using boron doped diamond electrodes for wastewater treatment. Electrochimica Acta 2004; 49 (9-10): 1587-1595. doi: 10.1016/S0013-4686(03)00966-6

40. Standards BI. Determination of cartap hydrochloride content (spectrophotometric method) copyrighted by Bureau of Indian Standards," IS 141591994.

41. Lee SJ, Caboni P, Tomizawa M, Casida JE. Cartap hydrolysis relative to its action at the insect nicotinic channel. Journal of Agricultural and Food Chemistry 2004; 52 (1): 95-98. doi: 10.1021/jf0306340

42. Zhang F, Sun Z, Cui J. Research on the mechanism and reaction conditions of electrochemical preparation of persulfate in a split-cell reactor using BDD anode. RSC Advances 2020; 10 (56): 33928-33936. doi: 10.1039/D0RA04669H

43. Wang HW, Bringans C, Hickey AJR, Windsor JA, Kilmartin P et al. Cyclic Voltammetry in Biological Samples: A Systematic Review of Methods and Techniques Applicable to Clinical Settings. Signals 2021; 2 (1): 138-158. doi: 10.3390/signals2010012

44. Liu Z, Ding H, Zhao C, Wang T, Wang P et al. Electrochemical activation of peroxymonosulfate with ACF cathode: Kinetics, influencing factors, mechanism, and application potential. Water Research 2019; 159: 111-121. doi: 10.1016/j.watres.2019.04.052

45. Hoang NT, Nguyen XC, Le PC, Juzsakova T, Chang SW et al. Electrochemical degradation of pesticide Padan 95SP by boron-doped diamond electrodes: The role of operating parameters. Journal of Environmental Chemical Engineering 2021; 9 (3): 105205. doi: 10.1016/j.jece.2021.105205

46. Lei Y, Lu J, Zhu M, Xie J, Peng S et al. Radical chemistry of diethyl phthalate oxidation via UV/peroxymonosulfate process: Roles of primary and secondary radicals. Chemical Engineering Journal 2020; 379: 122339. doi: 10.1016/j.cej.2019.122339

47. Lian L, Yao B, Hou S, Fang J, Yan S et al. Kinetic study of hydroxyl and sulfate radical-mediated oxidation of pharmaceuticals in wastewater effluents. Environmental Science & Technology 2017; 51 (5): 2954-2962. doi: 10.1021/acs.est.6b05536

48. W. Li, T. Jain, K. Ishida, H. Liu. A mechanistic understanding of the degradation of trace organic contaminants by UV/hydrogen peroxide, UV/persulfate and UV/free chlorine for water reuse. Environmental Science: Water Research & Technology 2017; 3 (1): 128-138. doi: 10.1039/C6EW00242K

49. Hoang NT, Nguyen VT, Tuan NDM, Manh TD, Le PC et al. Degradation of dyes by UV/Persulfate and comparison with other UV-based advanced oxidation processes: Kinetics and role of radicals. Chemosphere 2022; 298: 134197. doi: 10.1016/j.chemosphere.2022.134197

50. Cai J, Zhou M, Pan Y, Du X, Lu X. Extremely efficient electrochemical degradation of organic pollutants with co-generation of hydroxyl and sulfate radicals on Blue-TiO2 nanotubes anode. Applied Catalysis B: Environmental 2019; 257: 117902. doi: 10.1016/j.apcatb.2019.117902

51. Ji Y, Shi Y, Wang L, Lu J. Denitration and renitration processes in sulfate radical-mediated degradation of nitrobenzene. Chemical Engineering Journal 2017; 315: 591-597. doi: 10.1016/j.cej.2017.01.071

52. Buxton GV, Greenstock CL, Helman WP, Ross AB. Critical Review of rate constants for reactions of hydrated electrons, hydrogen atoms and hydroxyl radicals (·OH/·O − in Aqueous Solution. Journal of Physical and Chemical Reference Data 1988; 17 (2): 513-886. doi: 10.1063/1.555805

53. Neta P, Huie RE, Ross AB. Rate Constants for reactions of inorganic radicals in aqueous solution. Journal of Physical and Chemical Reference Data 1988; 17 (3): 1027-1284. doi: 10.1063/1.555808

54. Tan C, Jian X, Wu H, Sheng T, Sun TK et al. Kinetics degradation of phenacetin by solar activated persulfate system. Separation and Purification Technology 2021; 256: 117851. doi: 10.1016/j.seppur.2020.117851

55. Serrano K, Michaud PA, Comninellis C, Savall A. Electrochemical preparation of peroxodisulfuric acid using boron doped diamond thin film electrodes. Electrochimica Acta 2002; 48 (4): 431-436. doi: 10.1016/S0013-4686(02)00688-6

56. Ahna YY, Bae H, Kim HI, Kim SH, Kim JH et al. Surface-loaded metal nanoparticles for peroxymonosulfate activation: Efficiency and mechanism reconnaissance. Applied Catalysis B: Environmental 2019; 241: 561-569. doi: 10.1016/j.apcatb.2018.09.056

57. Davis J, Baygents JC, Farrell J. Understanding persulfate production at boron doped diamond film anodes. Electrochimica Acta 2014; 150: 68-74. doi: 10.1016/j.electacta.2014.10.104

58. Khamis D, Mahé E, Dardoize F, Devilliers D. Peroxodisulfate generation on boron-doped diamond microelectrodes array and detection by scanning electrochemical microscopy. Journal of Applied Electrochemistry 2010; 40 (10): 1829-1838. doi: 10.1007/s10800-010-0114-x